Hematite surface modification toward efficient sunlight-driven water splitting activity: Role of gold nanoparticle addition

Aryane Tofanello[1], Andre L. M. Freitas[1], Waldemir M. Carvalho-Jr[1], Turkka Salminen[2], Tapio Niemi[2] and Flavio L. Souza[1]*

[1] Laboratory of Alternative Energy and Nanomaterials, Universidade Federal do ABC, Sao Paulo, Brazil.

[2] Photonics Laboratory, Tampere University, Tampere, Finland.

Corresponding author
flavio.souza@ufabc.edu.br; fleandro.ufabc@gmail.com

Abstract

Localized surface plasmon resonance (LSPR) have been investigated to enhance light harvesting on hematite-based photoelectrode modified with AuNP, meanwhile, an extensive understanding about the different processes involved in hematite-AuNP system remains unclear. This work addresses a majority effect associated with AuNP-addition by comparing charge transfer, catalytic and light harvesting efficiencies. The obtained results revealed that the lower AuNP-amount leads to higher photocurrent response of 1.20 mA cm^{-2} at 1.23 V_{RHE} in comparison with all photoelectrodes designed here. Notoriously, increasing AuNP-amount supported on hematite surface clearly promoted higher light absorption, which was surprisingly not followed by photoelectrochemical efficiency. This result suggests here that the plasmon-effect is not a dominant phenomenon that drives the photoelectrode performance. In fact, the deeper analysis showed that the Schottky contact provides the Fermi level equilibration enhancing charge transport efficiency classifying as predominant effect to enhance photoresponse in the system.

Keywords: hematite-AuNP, plasmonic particle, charge transport, photoelectrochemical efficiency.

1. Introduction

The widely investigated photoelectrode-based hematite (α-Fe_2O_3) for water splitting faces some adversities hiding its performance such as: poor charge mobility, high electron-hole recombination rate and slow surface kinect. These limitations have sluggish oxygen-evolution kinetics and have decreased the efficiency of hematite photoelectrodes to date. Several strategies has been employed to overcome these intrinsic limitations and modify the electronic properties by depositing passivation layers,[1,2] incorporation of metal nanoparticles[3–5] and oxygen-evolution cocatalysts[6,7]

Hematite-based photoelectrodes with plasmonic nanoparticles showed a promisor results on the literature dealing with the localized surface plasmon resonance (LSPR).[8,9] Au nanoparticles (AuNP) stands up to recover the hematite photoelectrocatalytic efficiency rising to plasmonic light trapping in the hematite/electrolyte interface which contributes to charge separation. Some processes can be associated to hematite-AuNP interface[10]: (i) transport facilitated by Schottky junction leading with the Fermi-level equilibrium, promoting an enhanced charge transfer in between AuNP-hematite contact, (ii) passivated surface states induced by AuNPs contributing to reduce surface recombination, (iii) induced co-catalyst state improving surface kinect at solid-liquid interface and/or (iv) plasmon-enhanced hematite absorption. Additionally, it has been observed that metallic nanoparticles can easily oxidize their surface during the photocatalytic process and thus might not be chemically sustained in use for longer time.[11,12] Indeed, AuNP-modified surface can play different roles and an effective route to overcome the shortcomings of plasmonic metal nanoparticles on semiconductors in terms of energy transfer, scattering and hot electron transfer might be necessary to reduce recombination losses.[4,13–16] Despite the progress on understanding the role of AuNP over hematite system, it is clear that the water splitting

efficiency contributions by designing AuNP-modified hematite photoelectrodes remains a challenge in the state-of-art.[17]

In this scenario, this current work attempted to elucidate the limitations in the efficient charge transfer by varying the amount of AuNP deposited over hematite photoelectrodes to reveal the effective metallic particle charge transport mechanism clarifying the limiting and mandatory processes in this system. A proposed mechanism aligned to deeper investigation of photoelectrochemical properties and the characteristics of AuNP over hematite electrodes has been conducted. In summary, it was showed a synergetic effect addressed in between particles amount and AuNP-oxidize surface as the hard task to improve the system hematite-AuNP instead of absorption efficiency aggregated by plasmonic particle.

2. Experimental Methods

2.1 Materials Details

Fluorine-doped tin oxide (FTO, Solaronix RΩ~8-10 Ω cm−1, Transmission > 80% from 500 to 800 nm) substrate was used for growth of the hematite photoelectrodes. All chemicals were used without further purification. Iron (III) chloride ($FeCl_3$ $6H_2O$, 99%) and urea (NH_2CONH_2, 99.8%) were purchased from Sigma-Aldrich and Merck, respectively. The AuNPs in isopropanol (CAS number 7440-57-5, <20nm at 100mg/L, surfactant and reactant-free) were purchased from Strem Chemical.

2.2 Photoelectrode Synthesis procedure

Hematite photoelectrodes were grown onto FTO by aqueous route under hydrothermal condition.[18] For that, FTO substrates were separately cleaned by deionized water, ethyl alcohol and acetone solutions. The method consists in preparing 100 ml of aqueous solution of iron (III) chloride 1.5 10^{-3} mol L^{-1} and urea 1.5 10^{-3} mol L^{-1}. The system was subjected to hydrothermal conditions for

0.5, 1 or 2 hours in an oven (Memmert, Universal Oven UF 55) at 100 °C. After synthesis, the films were annealed in a tubular furnace (Carbolite) at 750 °C for 30 minutes with a heating rate of 3 °C min^{-1} and cooling rate of 1 °C min^{-1} to obtain the pure hematite films. The AuNP modifications were carried by a self-made dip coating system under several different conditions varying the amount of AuNP deposited: 1%, 2% and 4%. In a conventional route, AuNPs isopropanol solution (< 20nm at 100mg/L) was dip coated onto the surface of hematite photoelectrodes at a withdrawal speed of 0.03 mm min^{-1}. The samples were divided into two main groups: i) fixed hematite thickness, hydrothermally synthesized for 1h (H1: 237 ± 9 nm) varying the AuNP amount deposited, where, H1 (control sample, without AuNPs deposition), H1AuNP 1%, H1AuNP 2% and H1AuNP 4%; (ii) hematite photoelectrodes were synthesized in three different synthesis times (0.5, 1 and 2h) followed by deposition of a fixed amount of AuNP by dip coating maintaining the AuNP % deposited (AuNP 1%), which will be named H0.5AuNP 1%, H1AuNP 1% and H2AuNP 1%. The AuNP concentration (1, 2 or 4%) deposited in each sample was determined by successive large area top-view scanning electron microscopy (SEM) images and energy-dispersive X-ray spectroscopy (EDX) analyzes.

2.3 Characterizations Information

Morphological analysis was evaluated by SEM technique using a microscopy (FEG-SEM, FEI Inspect F50) in top and cross-sectional view. Additionally, the chemical map confirmed the elemental distribution using energy-dispersive X-ray spectroscopy (EDX) analysis. Optical absorbance/transmission measurements were carried out using a spectrophotometer (Cary 50 Conc UV/Vis spectrophotometer, Agilent, USA) without an integration sphere. Photoelectrochemical measurements were carried out with a scanning potentiostat (Potentiostat/Galvanostat μAutolab III with Fra module) in a three-electrode configuration with 1 M NaOH (pH 13.6) as the electrolyte

and an Ag/AgCl (in saturated KCl solution) reference electrode and platinum wire counter electrode. The measurements were performed in dark and under illumination with a solar simulator (450 W xenon lamp (Osram, ozone free) and an AM 1.5 filter). The light intensity was set to 100 mW cm^{-2}. Electrochemical impedance spectroscopy measurements were recorded in dark at open circuit potential over a frequency ranging from 10^5 to 0.1 Hz with amplitude of 10 mV. Mott-Schottky plots were obtained at a fixed frequency of 1 kHz.

Topographic and 3D images were obtained using an Atomic Force Microscopy (AFM, Agilent 5500) in tapping mode. It was used a cantilever with a spring constant of 42 N/m (manufacturer data) with a resonant frequency of 278 kHz. The acquisition of images was performed with a scan area of 4 x 4 μm^2. X-ray absorption near-edge structure (XANES) was performed at the Fe K-edge (7112eV eV) in the XAFS1 beamline of the Brazilian Synchrotron Light Laboratory (LNLS). To provide good energy reproducibility during data collection, the XANES spectrum of FeO standard or α-hematite standard was simultaneously measured, and the energy was calibrated by aligning the respective absorption edges. Data edge-step normalization was performed after a linear pre-edge subtraction and the regression of a quadratic polynomial beyond the edge, using ATHENA software FeO and hematite standards samples will be used as standards for Fe^{2+} and Fe^{3+} valence states, respectively. All standards samples were purchased from Sigma-Aldrich.

3. Results

Chemical method combined to an annealing procedure provide bare hematite electrodes with columnar morphology as illustrated in scanning electron microscopy (SEM) images, Figure 1. By playing with synthesis time (0.5, 1 and 2h), different hematite rods length or film thickness were estimated by cross-sectional SEM images, ranging from 140 to 380 nm (see Figure 1a-c).

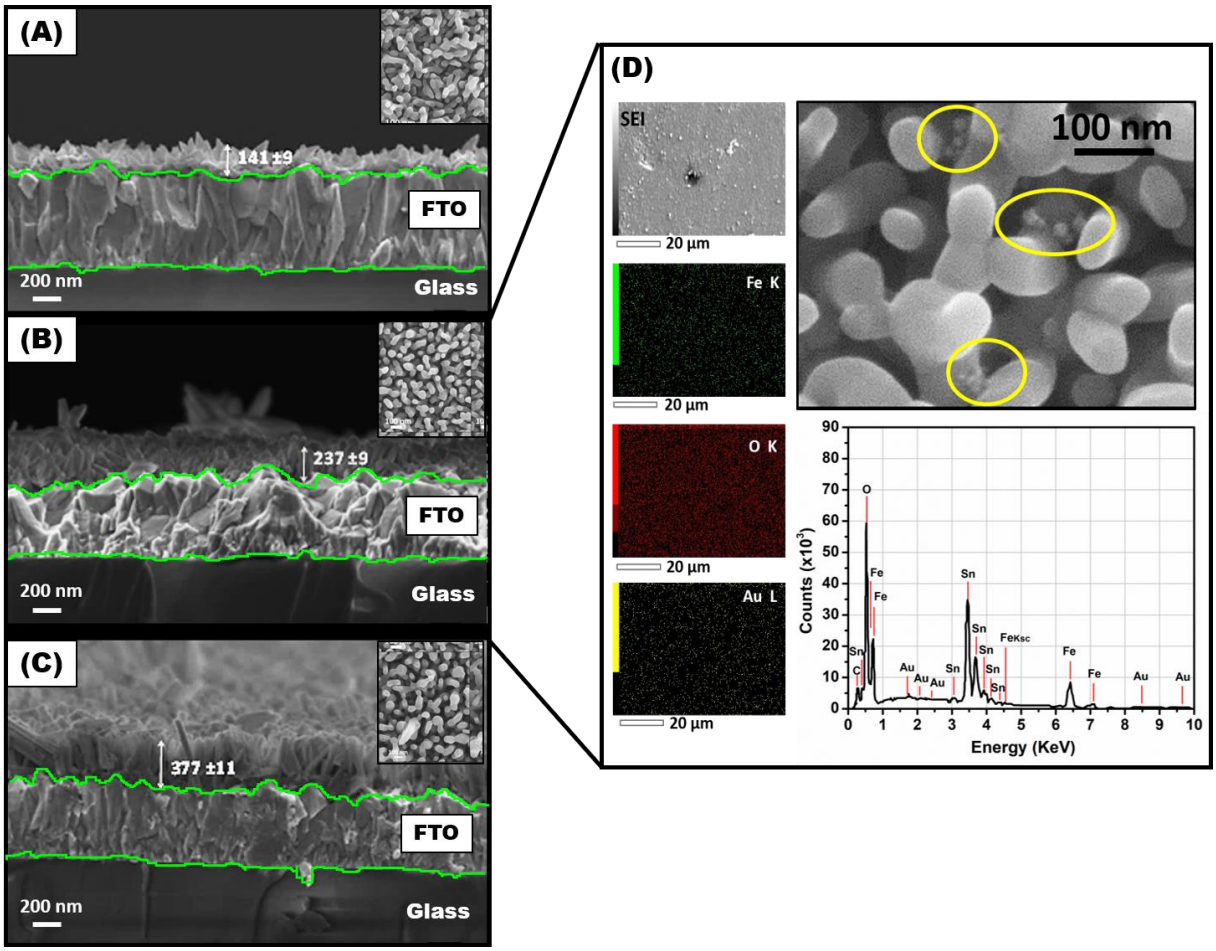

Figure 1. Scanning electron microscopy (SEM) images of cleaved hematite electrode synthesized with different thickness controlled by the substrate kept under hydrothermal conditions at constant temperature (100^{o} C): (a) 0.5 hour, (b) 1.0 hour and (c) 2.0 hours. (d) Top-view SEM images of gold nanoparticle AuNP-modified hematite photoelectrode and chemical map revealing the presence of those added particles (the AuNPs are highlighted in yellow).

The investigation was conducted to find the optimum performance of bare hematite electrode modified with gold nanoparticles (AuNPs). Hematite rods surface (Figure 1d) modification was done using the dip coating technique as described in experimental section. In this sense, two different approaches were performed: (i) fixed amount of AuNPs over all synthesized hematite electrode with different thickness (Figure 2a) and (ii) different AuNP concentration added over the

selected bare hematite electrode surface (Figure 2b). The AuNP modification was confirmed by SEM analysis and the additional chemical map (region highlighted by yellow circles) in Figure 1d without alter the nanorods morphology. By performing photoelectrochemical in triplicate measurements was selected the electrode for each condition mentioned in Experimental Section under front (Figure 2c - top) and back illumination (Figure 2c - down). The combination of the three different hematite thicknesses (synthesis time) with the three concentrations of AuNP deposition was summarized in terms of photocurrent response at 1.23 V_{RHE}.

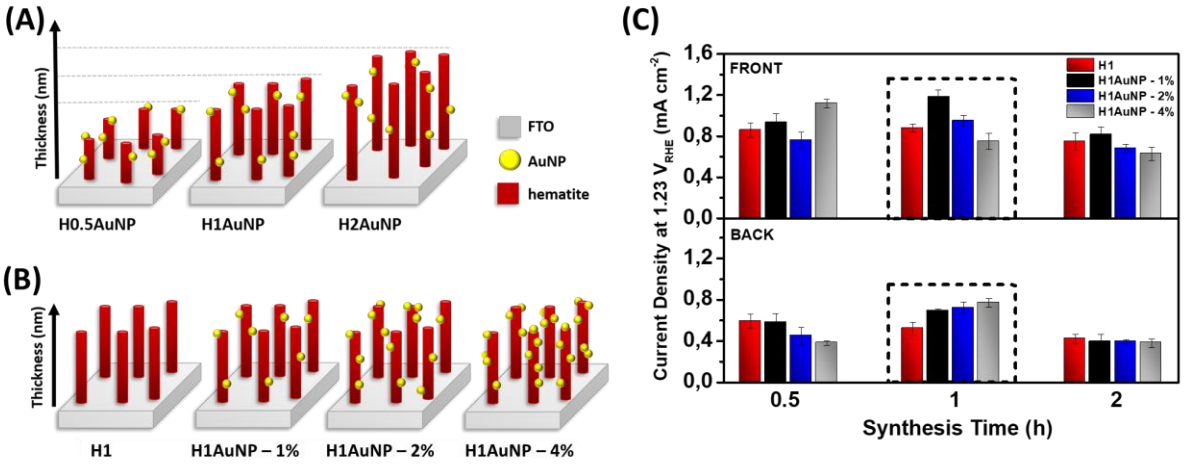

Figure 2. Schematic performed synthesis with: (A) fixed amount of AuNP varying hematite thickness and (B) fixed hematite thickness at 1h-hydrothermally synthesized (H1) varying AuNP concentration (1-4%); (C) Average photocurrent density at 1.23 V_{RHE} against synthesis time measured under front-side and back-side illumination. Red column: pure hematite, black column: hematite modified with 1% of AuNP, blue column: hematite modified with 2% of AuNP and gray column: hematite modified with 4% of AuNP.

Pure hematite photoelectrode in which no AuNP was deposited is taken as standard for reference comparison. The photocurrent responses at 1.23 V_{RHE} suggest that independent of the sunlight irradiation side and AuNP concentrations the highest performance can be achieved by electrodes

obtained after 1 hour of synthesis (see highlighted in black dashed square, Figure 2c). In addition, atomic force microscopy analysis conducted to all electrodes clearly shows that the 1 hour designed system (with and without AuNP) provides the highest available surface area-roughness combination (Figure S1, see supplementary information). Towards to understanding the role of metallic AuNP deposited on top of hematite surface electrodes the discussion will be focused on electrodes designed at 1 hour of synthesis (see schematic representation in Figure 2c). Firstly, the complete *JV* curve under front-side sunlight irradiation, presented in the supplementary data (Figure S2), was re-analyzed showing that the highest photocurrent response was achieved with low amount of AuNP (H1AuNP-1%) loaded. To address the photocatalytic improvement AuNP-induced on hematite electrodes, further analysis was conducted to understand the role of this semiconductor modification.

As a first step of analysis, the addition of AuNP over H1 photoelectrode surface was evaluated in terms of optical property by performing UV-visible spectroscopy. The transmittance spectra of pure hematite (H1) and decorated hematite photoelectrodes (H1AuNP 1 to 4%) were presented on Figure S3a. The transmittance curves showed a slightly decrease at all wavelengths for H1AuNP 1 and 2% in comparison to the H1 spectra. However, H1AuNP 4% exhibited a pronounced reduction in the transmittance profile which is probably related to the highest amount of AuNP deposited. Considering that the hematite thickness is the same for all photoelectrodes analyzed, the increase in the light absorption was calculated by subtracting the absorption curve of AuNP-containing photoanodes with that of pure hematite. Once the contribution of hematite phase is extracted from optical absorption spectra, it was possible to observe an enhancement in absorption along the wavelength from 500 to 600 nm, which is the typical absorption band for the SPR effect of AuNP (Figure S3b). AuNP solution absorption spectra was included as control and characteristic absorption peak was centered at around 530 nm for the AuNPs with average size of 20 nm, as seen

in Figure S3b (black dotted line). Red-shift on the AuNP characteristic peak for the hematite-modified photoelectrodes was observed due to the coupling between the metal and semiconductor. Besides that, plasmon absorption peak wavelength is affected by the amount of AuNP and the red shift might be a consequence of a high number of deposited particles, suggesting an agglomerated AuNPs on hematite surface.[19,20] This effect is clearly noticed for H1AuNP 4%, which presented a broader plasmon band, supporting the agglomerated prediction and evidencing that high AuNP concentrations can affect the photoelectrochemical performance.

Following step was conducting electrochemical impedance spectroscopy under dark (EIS) and illuminated condition (PEIS) to get insights on the electronic parameters with presence of AuNP over hematite photoelectrode. EIS and PEIS data were analyzed in terms of Mott-Schottky plots were the linear adjustment analyzed at frequency of 1 KHz allowed to estimate electronic parameters which was summarized on Table 1. The results revealed no significant changes on the overall capacitance represented by the slope at the Mott-Schottky plots (Figure S4).

Table 1. Current density measured at 1.23 V_{RHE} and electrochemical parameters calculated from Mott-Schottky linear adjustment in a presence and absence of sunlight simulated conditions: donors density (N_D), flat band potential (V_{fb}) and depletion layer length (W).

	***J* at 1.23 V_{RHE} (mA cm^{-2})**	**N_D (10^{19} cm^{-3})**		**V_{fb} (V_{RHE})**		**W (nm)**	
		Dark	*Light*	*Dark*	*Light*	*Dark*	*Light*
H	0.82	5.38	5.41	0.43	0.36	14	13
H1AuNP 1%	1.20	4.70	4.89	0.54	0.42	16	16
H1AuNP 2%	0.95	3.63	3.52	0.53	0.41	18	16
H1AuNP 4%	0.75	6.00	4.05	0.49	0.39	16	16

EIS/PEIS (Figure S4a-d) and calculated parameters does not confirm that the major effect of AuNP-incorporation is associated to electronic effect inducing enhancement on photoelectrocatalytic performance. Similarly, Li et al[10] reported a negative shift in the flat-band potential from 0.32 V_{RHE} for bare hematite to 0.20 V_{RHE} for hematite-AuNP and the Mott-Schottky slope was bit smaller AuNP-modified electrode, indicating higher capacitance on the interface. On the other hand, the authors showed that after performing a protective layer on the AuNP surface the flat-band potential returns to 0.31 V_{RHE}. The negative shifts on the onset potential for Li's work suggests the catalytic nature of those AuNP.

In our work N_D, V_{fb} and W values were not significantly affected by AuNP presence on hematite surface in light conditions which does not explain the difference on the photocurrent changes. At this point, we can confirm that the metallic particle is forming a heterojunction onto the surface. Although, it was noticed (Figure S4 a and c) an increase in the resistance to charge transfer aligned to the increased AuNP amount in Nyquist plots. This confirms the presence of a heterojunction forming a Schottky-layer increasing the charge distribution in between hematite-AuNP contact which is a new resistance is associated to the system.

Besides the disparity observed in optical properties, photoelectrochemical performance and no clear electronic effect for AuNP-added at fixed hematite thickness, a further discussion about the efficiency is helpful to clarify the obtained results. Considering the global photoelectrochemical efficiency as a function of absorption (Jabs), catalytic (η_{cat}) and charge separation efficiency (η_{sep}), the photo-response can be written as Equation 1 below:

$$J_{photo} = J_{abs} \cdot \eta_{cat} \cdot \eta_{sep} \quad (1),$$

where the J_{abs} is function of the integrated absorption spectra, η_{cat} is represented by the ratio in between the photocurrent obtained in alkaline electrolyte and photocurrent resulted from OH-

saturated electrolyte (J_{photo}/J_{H2O2}), and n_{sep} = J_{H2O2}/J_{abs}, as defined elsewhere.[21,22] Figure 3 summarizes the global equation parameters and analysis.

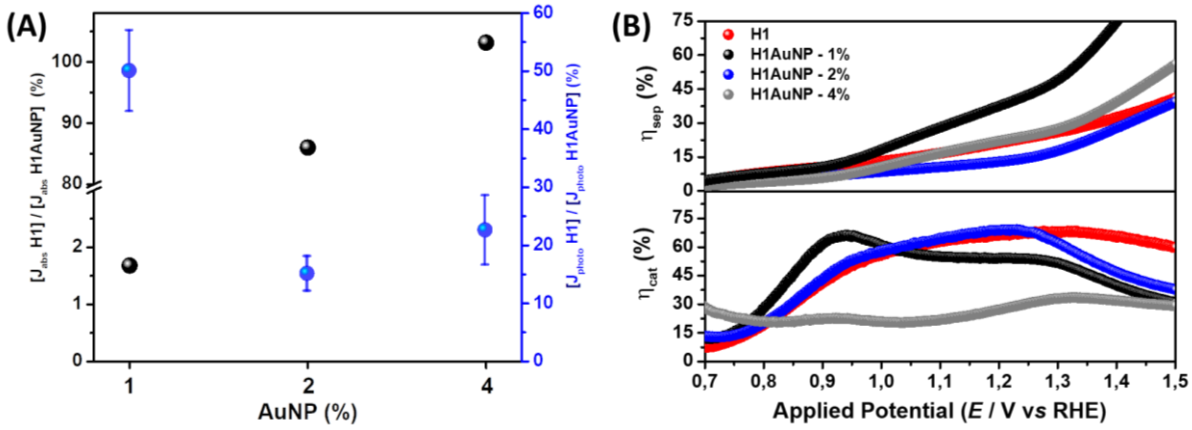

Figure 3. (A) Increment of absorption and measured photocurrent on the unmodified hematite related to AuNP-deposited amount; (B) Separation (top) and catalytic (down) efficiencies calculated from experimental data for each condition.

Figure 3a revealed the contributions on hematite J_{abs} due to incorporation of AuNP, where was noticed a linear enhancement on hematite J_{abs} increasing due the concentration of AuNP, as discussed on optical analysis. This linear enhancement can be confirmed once the hematite layer thickness was fixed and no additional annealing was performed after AuNP deposition. On another hand, the linearity observed on absorption efficiency was not followed on photocurrent response. The lowest absorption contribution was found for H1AuNP 1% which reached 1.5% of increment in the J_{abs} parameter. In contrast, the global efficiency does not show this trend where the photocurrent density was enhanced to about ~50% for H1AuNP 1%, followed by ~15-20% for H1AuNP 2% and H1AuNP 4%, in comparison with bare photoelectrodes. This result suggests that

the photoelectrochemical enhancement might be contribution of another parameter which is not majority related to plasmon-effect.

Furthermore, the catalytic and separation efficiency were illustrated on Figure 3b. As evidenced by LSV measurement (Figure S2), H1AuNP 1% acts specifically in photocurrent evolution at potentials higher than 1.0 V_{RHE}. In fact, the charge transport was enhanced, highlighted by the difference on separation efficiency (Figure 3b – top). On the other hand, the incorporation of AuNP does not contribute to the catalytic efficiency at potentials higher than 1.0 V_{RHE} independent of the AuNP amount, as observed on Figure 3b-down. The result clarifies that the major effect on surface modification is attributed to charge transport efficiency. Therefore, the remaining question that arises is regarding to the mechanism that governs the charge transfer on AuNP-modifying hematite during photoelectrochemical measurements.

What is the mechanism for charge transfer on hematite-AuNP electrode?

Further experiments to help us to address this question was carried out. X-ray absorption near-edge structure (XANES) was used to investigate and clarify the effect of the AuNP 1% on the hematite surface. The data revealed the fingerprint of the phases and valence states, where Figure 4 shows the normalized XANES spectra recorded at the Fe K-edge of iron-containing chemical standards (FeO (Fe^{2+}) and α-hematite (Fe^{3+})) and H1AuNP 1% photoelectrode. It is evident in Figure 4 that the XANES spectra profile of hematite standard and H1AuNP 1% are significantly different from that obtained for the FeO. Two distinct regions at low (LE) and high (HE) energy is observed, which is a characteristic behavior found for iron-based materials. LE-region in XANES spectra correspond to the pre-edge, which showed a similar profile for α-hematite standard and H1AuNP 1% manifesting the presence of Fe^{3+} species in the samples.[23] The Fe K-edge absorption energies

in LE region appear at 7112.5 and 7115 for FeO, hematite and H1AuNP 1%, respectively, as was expected (no anomalous structural behavior).

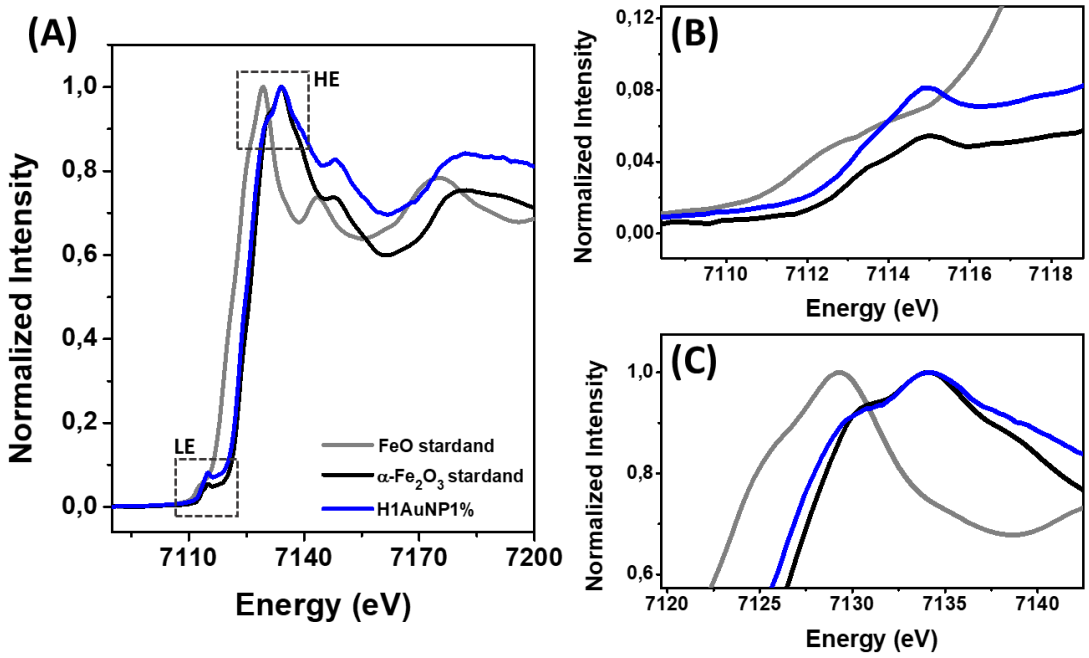

Figure 4. (A) Normalized XANES spectra at the Fe-K absorption edge of the FeO standard, hematite standard and H1AuNP 1%; Zoom-view at (B) Low-energy region (LE) and (C) High-energy (HE) region.

According to previous reports and comparison with the α-hematite standard spectrum, the first peak centered around 7115 eV is associated with local excitations of 1s electrons to d levels.[24] Although the position of the pre-edge peak is very sensitive to changes in speciation, oxidation, and coordination states (in particular to the Fe^{3+}/total Fe ratio), its intensity showed no variation in H1AuNP 1%, which means that Fe-d levels were not nearly disturbed by the presence of the metal.[25,26] The Fe species in the AuNP-modified photoelectrodes were mainly present in the form of Fe^{3+}, similar to bare hematite.[27]

Thus, the slight spectral change of Fe L-edge (Fig 4) suggests the chemical interaction between the semiconductor and metallic nanoparticles, probably promoting the charge transfer from Fe (3d) state to Au (6s/5d) due to orbital interaction.[28] This may lead to increased oxygen electrocatalysis,

causing the plasmonic layer to act in the evolution of the as water oxidation. [29] The second region (HE), considered as main edge, verifies the effect of the AuNP deposition on the photoelectrodes. Based on XANES data, it was possible to observe the differences in between the pure hematite surface and the modified ones with AuNPs, suggesting the advantage of the semiconductor + metal assembly for PEC devices. The sample H1AuNP 1% presented a well-defined shoulder around 7130 eV and the peak of maximum energy at 7134 eV, which is due to the dipole-allowed 1s to 4p electron transition, similar to the hematite standard.[25] As the intensity of the 1s to 4p transition was proportional to the population of Fe(III), it is possible to conclude that the H1AuNP 1% photoelectrode has less iron ions in the Fe^{3+} valence state.[30]

X-ray photoelectron spectroscopy (XPS) was performed to detail the surface chemistry of AuNP anchored over hematite photoelectrodes, as seen in the Figure 5.

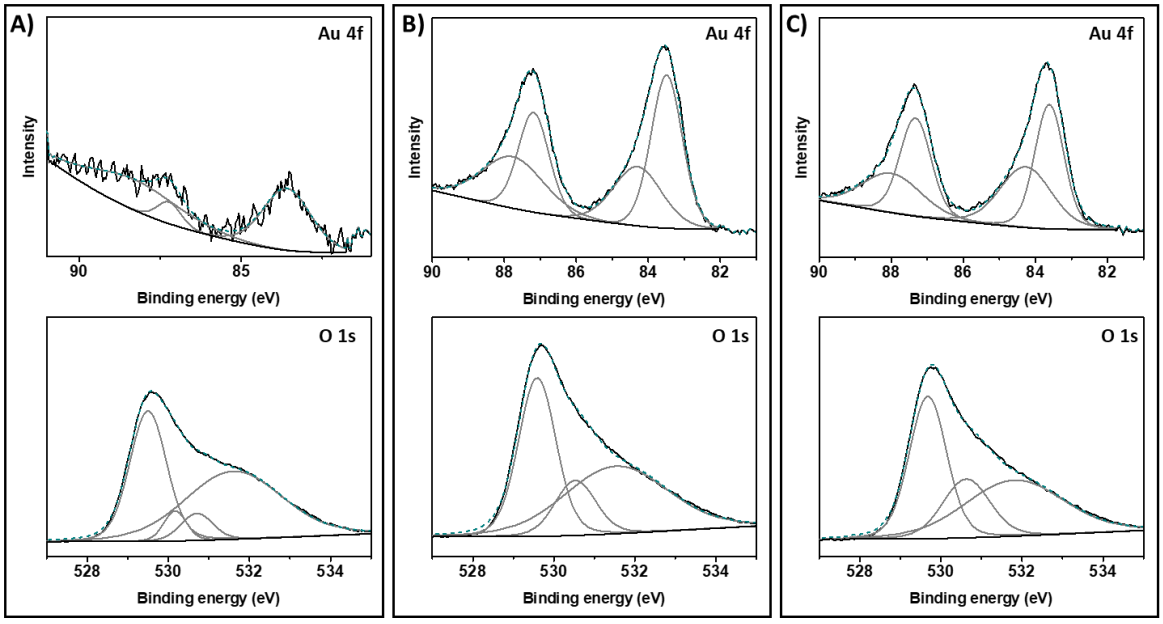

Fig 5. XPS profile of Au 4f (top) and O 1s (down) after photo-electrochemical measurements: (A) H1AuNP 1%, (B) H1AuNP 2% and (C) H1AuNP 4%.

XPS data illustrated that the AuNP, after photoelectrochemical measurements at alkaline electrolyte, undergo partially electrochemical oxidation. A high-resolution spectrum of Au4f, shown in the top Fig 5 a-c, contains peaks due to different gold oxidation states (Au^0 and $Au^{+\delta}$ where δ=variable gold oxidation state).[31] The Au 4f spectra of the hematite-modified photoelectrodes show a signed metallic peak (Au^0) at a binding energy of 83.6 eV with an orbital split pronounced at 87.5 eV. It was clearly noticed that H1AuNP 4% has a higher amount of Au nanoparticles compared H1AuNP 1%. The existence of an additional pair was interpreted as the state of oxidized gold complexes ($Au^{+\delta}$), which is assigned to the presence of small amounts of gold oxygen compounds on the gold nanoparticle surface as a result of gold oxidation during photoelectrochemical processes[32,32–34] This result supports the formation of a thin layer of gold complex covering the AuNPs, since at high potentials and alkaline media the formation of oxidized gold species may takes place.[35] Thus, based on thermodynamic stability, we proposed that the surface consists of an overlayer oxygen being chemically absorbed on AuNP. [36–38] Previous studies, under different experimental conditions, have been able to distinguish different Au-O species based on the contribution of various peaks in their O 1s XPS spectra.[36,39] The same analysis and interpretation cannot be done because AuNPs are deposited on the hematite and the overlap between the binding energies of the different oxide species makes their individual detection difficult , so the different Au-O/Au-OH complexes are not easily distinguished based on the XPS spectra of the Au 4f region.[35,39,40] Despite this limitation, the O 1s spectra show changes in the energetic state of the 1s oxygen electrons on the different AuNP-hematite systems, suggesting the presence of several oxygen species and supporting the hypothesis of the presence of an oxidized gold complex layer. [36,39,41]

General Discussions

Overall enhancement on photoelectrocatalytic performance can be assigned to amount of AuNP added on top of hematite photoanode. The electrochemical characterizations suggested that H1AuNP 1% enhances surface electron transfer at the photoanode/electrolyte interface. Three hypotheses are commonly addressed to explain the origin of the enhanced surface charge transport by AuNPs in contact with semiconductor: (i) increased charge transfer from semiconductor-to-electrolyte facilitated by metallic nanoparticle presence (co-catalyst effect)[29,42] (ii) AuNPs acting as a passivating layer, which leads to a reduction of the surface recombination[43] and (iii) plasmon-enhanced hematite absorption.

Based on our results, AuNPs plasmon resonance has showed optical absorption influence in our photoelectrodes in the visible range but it is clearly that it is not determinant to the hematite photoelectrochemical performance. In this same direction, Li's report showed that the main effects is based to Fermi level equilibration and surface catalysis with low-contribution on photoelectrochemical response provided by plasmonic effect.[10] In this case, a schematic photoelectrochemical process at AuNP-modified photoelectrodes interface indicating the limitations involved in the photocatalytic processes was proposed in Figure 6.

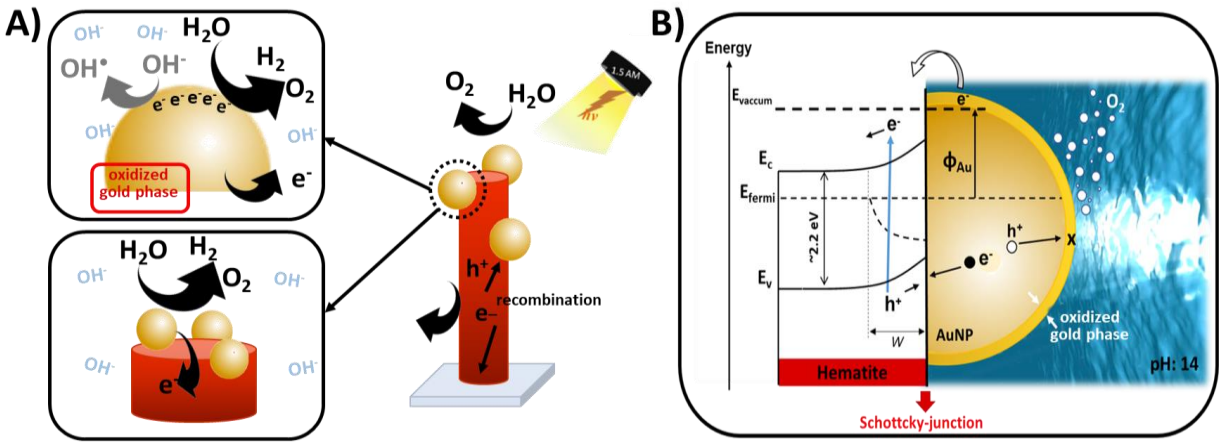

Figure 6. Schematic representation of (A) AuNP/hematite/electrolyte interface in the photoelectrochemical conditions and (B) band diagram.

Figure 6a summarizes the processes of photo-oxidation considering the AuNP in contact with the electrolyte under illumination. In this work we understand that multiples charge transfer processes can occur in the system, as evidenced in the band diagram (Figure 6b). The AuNP supported onto hematite photoelectrodes submitted to an alkaline medium and light-simulated conditions might deal with electrons being transferred from AuNP-to-semiconductor surface. The photogenerated holes created on the semiconductor surface can be trapped by generated states in the AuNP-hematite contact, as suggest in the schematic band diagram on Figure 6b.

The Schottky interface among AuNP-hematite electrodes corroborate to inject electrons directly in the hematite conduction band, improving the available charges (non-major effect) based on the Fermi Level equilibration. Although the limiting process is attributed to the transfer in the AuNP-electrolyte interface due to the oxidize resistive surface which contribute to enhance recombination (as shown on the XPS results and confirmed in the EIS-PEIS).

Due to the alteration of the electrochemical surface potential during the anodic process, AuNP oxidation is preferentially governed by O/OH adsorption and Au-O/OH place-exchange.[35] It is already known that the gold species rapidly hydrolyzes to form complexes on the AuNP surface during oxygen evolution process under highly alkaline medium.[44] From the extremely catalytic surface, the AuNP interact with hydroxyl groups and hematite surface leading to the formation of oxidized AuNP after photoelectrochemistry measurements.[39,45,46] The formation of unstable Au

hydroxide might be related to abundance OH* radicals from electrolyte which can oxidize metallic Au as clarified in the XPS profiles and similarly observed in the literature.[47,48]

Cyclic voltammetry measurements were performed to clarify the electrochemical effect on AuNP surface, and the electrodes was analyzed by UV-visible spectra, detailed on Figure S5. Au-modified photoelectrodes were subjected to 20 cycles ranging from -0.8 to 0.8 Ag/AgCl, and the results indicated that the applied potential and the interaction with the alkaline electrolyte lead to a slight oxidation of the AuNPs. The contribution of light in the formation of an oxidized product can also be seen in Figure S5. The appearance of this hydrated/oxidized gold phase in the interface electrode/electrolyte may affect the conductivity impairing the photocatalytic performance due to the passivation layer on the surface formation, decreasing the number of the transferred charge.[49] Most notably, it has been reported that the appearance of the oxidized gold species on metals can induce a reduction of the metal work function.[39,47,50] This implies that under photoelectrochemical conditions, the presence of chemisorbed species (Au-O) plays role in the photoactivity of AuNP. In this case, the oxidized gold phase acts as inhibitor for water oxidation as it is a non-photoactive material.

Based on the obtained results and return to band diagram (Figure 6b), it is possible to observe that the processes involved between the injection of electrons by the AuNP into hematite and the total interaction of the system with the electrolyte should be a synergy between: gold-amount and oxidized gold layer thickness. Thus, the encapsulation of the AuNPs should be necessary to reduce the effect of surface states induced by oxidized interface, as already proposed by other authors. In summary, the gain achieved in the water splitting efficiency with AuNP-hematite photoelectrodes is governed by a sum of factors, such as the thickness of nanorods, permeability of the electrolyte, roughness, and linearity in the deposition of AuNP. In this work the mandatory process to enhance

hematite-AuNP system photoelectrochemical performance is related to the increased charge transfer in the Schottky contact mediated by Fermi Level equilibration.

6. Conclusions

In summary, we demonstrated that the photoactivity of AuNP-hematite photoelectrodes for photoelectrochemical water oxidation can be effectively enhanced in the entire UV−visible region by adopting different amount AuNP deposited. The obtained results revealed that, differently of the commonly reported for hematite-AuNP system, the addressed absorption improvement was not the major mechanism responsible to contribute to the photoelectrochemical performance. The Schottky contact in between hematite-AuNP and the Fermi level equilibration provided an enhancement in the charge separation efficiency, leading to the conclusion that the enhanced transport is the majority of the effect to enhance photoresponse. Moreover, the AuNP-oxidized surface clarifies an important insight about the limiting process to achieve an improved catalytic efficiency on the solid-liquid interface. The controlled amount of deposited AuNP while maintaining a good surface catalysis is the determinant factor to improve photoelectrocatalytic performance.

7. Acknowledgements

We acknowledge the financial support from the Brazilian agencies FAPESP (Sao Paulo Research Foundation) (grant: 2014/50516-6) and Academy of Finland (collaborative research grant 2014/284652), CNPq, CAPES, and CEM-UFABC (Multiuser Experimental Center of Federal University of ABC). We also acknowledge Brazilian Synchrotron Light Laboratory (LNLS) for the beamline XFAS1 time and professor's Edson R. Leite group (LIEC – UFSCAR) for the SEM-EDX analyzes.

8. References

(1) Steier, L.; Herraiz-Cardona, I.; Gimenez, S.; Fabregat-Santiago, F.; Bisquert, J.; Tilley, S. D.; Grätzel, M. Understanding the Role of Underlayers and Overlayers in Thin Film Hematite Photoanodes. *Adv. Funct. Mater.* **2014**, *24* (48), 7681–7688. https://doi.org/10.1002/adfm.201402742.

(2) Gross Koren, M.; Dotan, H.; Rothschild, A. Nano Gold Rush: On the Origin of the Photocurrent Enhancement in Hematite Photoanodes Decorated with Gold Nanoparticles. *J. Phys. Chem. C* **2016**, *120* (28), 15042–15051. https://doi.org/10.1021/acs.jpcc.6b03735.

(3) Iandolo, B.; Antosiewicz, T. J.; Hellman, A.; Zorić, I. On the Mechanism for Nanoplasmonic Enhancement of Photon to Electron Conversion in Nanoparticle Sensitized Hematite Films. *Phys. Chem. Chem. Phys.* **2013**, *15* (14), 4947. https://doi.org/10.1039/c3cp44483j.

(4) Thimsen, E.; Le Formal, F.; Grätzel, M.; Warren, S. C. Influence of Plasmonic Au Nanoparticles on the Photoactivity of Fe 2O3 Electrodes for Water Splitting. *Nano Lett.* **2011**, *11* (1), 35–43. https://doi.org/10.1021/nl1022354.

(5) Wang, H.; Brandl, D. W.; Le, F.; Nordlander, P.; Halas, N. J. Nanorice: A Hybrid Plasmonic Nanostructure. *Nano Lett.* **2006**, *6* (4), 827–832. https://doi.org/10.1021/nl060209w.

(6) Sivula, K.; Le Formal, F.; Grätzel, M. Solar Water Splitting: Progress Using Hematite (α-Fe(2) O(3)) Photoelectrodes. *ChemSusChem* **2011**, *4* (4), 432–449. https://doi.org/10.1002/cssc.201000416.

(7) Kim, J. Y.; Youn, D. H.; Kang, K.; Lee, J. S. Highly Conformal Deposition of an Ultrathin FeOOH Layer on a Hematite Nanostructure for Efficient Solar Water Splitting. *Angew. Chemie - Int. Ed.* **2016**, *55* (36), 10854–10858. https://doi.org/10.1002/anie.201605924.

(8) Chaudhary, P.; Ingole, P. P. Multifunctional Plasmonic Ag-Hematite Nano-Dendrite Electro-Catalysts for Methanol Assisted Water Splitting: Synergism between Silver Nanoparticles and Hematite Dendrites. *Int. J. Hydrogen Energy* **2018**, *43* (3), 1344–1354. https://doi.org/10.1016/j.ijhydene.2017.10.136.

(9) Gao, H.; Liu, C.; Jeong, H. E.; Yang, P. Plasmon-Enhanced Photocatalytic Activity of Iron Oxide on Gold Nanopillars. *ACS Nano* **2012**, *6* (1), 234–240. https://doi.org/10.1021/nn203457a.

(10) Li, J.; Cushing, S. K.; Chu, D.; Zheng, P.; Bright, J.; Castle, C.; Manivannan, A.; Wu, N. Distinguishing Surface Effects of Gold Nanoparticles from Plasmonic Effect on Photoelectrochemical Water Splitting by Hematite. *J. Mater. Res.* **2016**, *31* (11), 1608–1615. https://doi.org/10.1557/jmr.2016.102.

(11) Wang, M.; Ye, M.; Iocozzia, J.; Lin, C.; Lin, Z. Plasmon-Mediated Solar Energy Conversion via Photocatalysis in Noble Metal/Semiconductor Composites. *Advanced*

Science. 2015. https://doi.org/10.1002/advs.201600024.

(12) Kazuma, E.; Sakai, N.; Tatsuma, T. Nanoimaging of Localized Plasmon-Induced Charge Separation. *Chem. Commun.* **2011**. https://doi.org/10.1039/c1cc10936g.

(13) Warren, S. C.; Thimsen, E. Plasmonic Solar Water Splitting. *Energy Environ. Sci.* **2012**, *5* (1), 5133–5146. https://doi.org/10.1039/c1ee02875h.

(14) Archana, P. S.; Pachauri, N.; Shan, Z.; Pan, S.; Gupta, A. Plasmonic Enhancement of Photoactivity by Gold Nanoparticles Embedded in Hematite Films. *J. Phys. Chem. C* **2015**, *119* (27), 15506–15516. https://doi.org/10.1021/acs.jpcc.5b02357.

(15) Thomann, I.; Pinaud, B. A.; Chen, Z.; Clemens, B. M.; Jaramillo, T. F.; Brongersma, M. L. Plasmon Enhanced Solar-to-Fuel Energy Conversion. *Nano Lett.* **2011**, *11* (8), 3440–3446. https://doi.org/10.1021/nl201908s.

(16) Lee, J. B.; Choi, S.; Kim, J.; Nam, Y. S. Plasmonically-Assisted Nanoarchitectures for Solar Water Splitting: Obstacles and Breakthroughs. *Nano Today*. 2017, pp 61–81. https://doi.org/10.1016/j.nantod.2017.08.008.

(17) Ding, C.; Shi, J.; Wang, Z.; Li, C. Photoelectrocatalytic Water Splitting: Significance of Cocatalysts, Electrolyte, and Interfaces. *ACS Catal.* **2017**, *7* (1), 675–688. https://doi.org/10.1021/acscatal.6b03107.

(18) Carvalho, W. M.; Souza, F. L. Hematite Surface Activation by Chemical Addition of Tin Oxide Layer. *ChemPhysChem* **2016**, 2710–2717. https://doi.org/10.1002/cphc.201600316.

(19) Liu, Y.; Xu, Z.; Yin, M.; Fan, H.; Cheng, W.; Lu, L.; Song, Y.; Ma, J.; Zhu, X. Enhanced Photoelectrocatalytic Performance of α-Fe 2 O 3 Thin Films by Surface Plasmon Resonance of Au Nanoparticles Coupled with Surface Passivation by Atom Layer Deposition of Al 2 O 3. **2011**. https://doi.org/10.1186/s11671-015-1077-y.

(20) Ma, Z.; Han, H.; Tu, S.; Xue, J. Fabrication of Shape-Controlled Hematite Particles and Growth of Gold Nanoshells. *Colloids Surfaces A Physicochem. Eng. Asp.* **2009**, *334* (1–3), 142–146. https://doi.org/10.1016/j.colsurfa.2008.10.015.

(21) Zandi, O.; Hamann, T. W. The Potential versus Current State of Water Splitting with Hematite. *Phys. Chem. Chem. Phys.* **2015**, *17* (35), 22485–22503. https://doi.org/10.1039/C5CP04267D.

(22) Nogueira, A. E.; Soares, M. R. S.; Souza Junior, J. B.; Ospina, C.; Souza, F. L.; Leite, E. R. Discovering a Selective Semimetal Element to Increase Hematite Photoanode Charge Separation Efficiency. *J. Mater. Chem. A* **2019**, *7* (28), 16992–16998. https://doi.org/10.1039/c9ta05452a.

(23) Yang, S.; Wang, D.; Liang, G.; Yiu, Y. M.; Wang, J.; Liu, L.; Sun, X.; Sham, T.-K. Soft X-Ray XANES Studies of Various Phases Related to LiFePO4 Based Cathode Materials. *Energy Environ. Sci.* **2012**, *5* (5), 7007. https://doi.org/10.1039/c2ee03445j.

(24) Chen, L. X.; Liu, T.; Thurnauer, M. C.; Csencsits, R.; Rajh, T. Fe 2 O 3 Nanoparticle Structures Investigated by X-Ray Absorption Near-Edge Structure, Surface Modifications, and Model Calculations. *J. Phys. Chem. B* **2002**, *106* (34), 8539–8546.

https://doi.org/10.1021/jp025544x.

(25) Ferraz, L. C. C.; Carvalho, W. M.; Criado, D.; Souza, F. L. Vertically Oriented Iron Oxide Films Produced by Hydrothermal Process: Effect of Thermal Treatment on the Physical Chemical Properties. *ACS Appl. Mater. Interfaces* **2012**. https://doi.org/10.1021/am301425e.

(26) Moog, I.; Feral-Martin, C.; Duttine, M.; Wattiaux, A.; Prestipino, C.; Figueroa, S.; Majimel, J.; Demourgues, A. Local Organization of Fe^{3+} into Nano-CeO_2 with Controlled Morphologies and Its Impact on Reducibility Properties. *J. Mater. Chem. A* **2014**, *2* (47), 20402–20414. https://doi.org/10.1039/C4TA02631D.

(27) Berry, A. J.; O'Neill, H. S. C.; Jayasuriya, K. D.; Campbell, S. J.; Foran, G. J. XANES Calibrations for the Oxidation State of Iron in a Silicate Glass. *Am. Mineral.* **2003**, *88* (7), 967–977. https://doi.org/10.2138/am-2003-0704.

(28) Shen, S.; Zhou, J.; Dong, C. L.; Hu, Y.; Tseng, E. N.; Guo, P.; Guo, L.; Mao, S. S. Surface Engineered Doping of Hematite Nanorod Arrays for Improved Photoelectrochemical Water Splitting. *Sci. Rep.* **2014**, *4*, 1–9. https://doi.org/10.1038/srep06627.

(29) Haro, M.; Abargues, R.; Herraiz-Cardona, I.; Martínez-Pastor, J.; Giménez, S. Plasmonic versus Catalytic Effect of Gold Nanoparticles on Mesoporous TiO2 Electrodes for Water Splitting. *Electrochim. Acta* **2014**, *144*, 64–70. https://doi.org/10.1016/J.ELECTACTA.2014.07.146.

(30) Lin, K. S.; Wang, Z. P.; Chowdhury, S.; Adhikari, A. K. Preparation and Characterization of Aligned Iron Nanorod Using Aqueous Chemical Method. *Thin Solid Films* **2009**, *517* (17), 5192–5196. https://doi.org/10.1016/j.tsf.2009.03.163.

(31) Tchaplyguine, M.; Mikkelä, M. H.; Zhang, C.; Andersson, T.; Björneholm, O. Gold Oxide Nanoparticles with Variable Gold Oxidation State. *J. Phys. Chem. C* **2015**. https://doi.org/10.1021/acs.jpcc.5b00811.

(32) Sylvestre, J. P.; Poulin, S.; Kabashin, A. V.; Sacher, E.; Meunier, M.; Luong, J. H. T. Surface Chemistry of Gold Nanoparticles Produced by Laser Ablation in Aqueous Media. *J. Phys. Chem. B* **2004**. https://doi.org/10.1021/jp047134.

(33) Klyushin, A. Y.; Rocha, T. C. R.; Hävecker, M.; Knop-Gericke, A.; Schlögl, R. A near Ambient Pressure XPS Study of Au Oxidation. *Phys. Chem. Chem. Phys.* **2014**. https://doi.org/10.1039/c4cp00308j.

(34) Li, Z.; Su, C.; Wu, D.; Zhang, Z. Gold Nanoparticles Decorated Hematite Photoelectrode for Sensitive and Selective Photoelectrochemical Aptasensing of Lysozyme. *Anal. Chem.* **2018**. https://doi.org/10.1021/acs.analchem.7b04015.

(35) Cherevko, S.; Topalov, A. A.; Zeradjanin, A. R.; Katsounaros, I.; Mayrhofer, K. J. J. Gold Dissolution: Towards Understanding of Noble Metal Corrosion. *RSC Adv.* **2013**, *3* (37), 16516. https://doi.org/10.1039/c3ra42684j.

(36) Juodkazis, K.; Juodkazyte, J.; Jasulaitiene, V.; Lukinskas, A.; Šebeka, B. XPS Studies on the Gold Oxide Surface Layer Formation. *Electrochem. commun.* **2000**. https://doi.org/10.1016/S1388-2481(00)00069-2.

(37) Shi, H.; Asahi, R.; Stampfl, C. Properties of the Gold Oxides Au2 O3 and Au2 O: First-Principles Investigation. *Phys. Rev. B - Condens. Matter Mater. Phys.* **2007**. https://doi.org/10.1103/PhysRevB.75.205125.

(38) Diaz-Morales, O.; Calle-Vallejo, F.; De Munck, C.; Koper, M. T. M. Electrochemical Water Splitting by Gold: Evidence for an Oxide Decomposition Mechanism. *Chem. Sci.* **2013**. https://doi.org/10.1039/c3sc50301a.

(39) Ono, L. K.; Roldan Cuenya, B. Formation and Thermal Stability of Au 2 O 3 on Gold Nanoparticles: Size and Support Effects. *J. Phys. Chem. C* **2008**, *112* (12), 4676–4686. https://doi.org/10.1021/jp711277u.

(40) Min, B. K.; Alemozafar, A. R.; Pinnaduwage, D.; Deng, X.; Friend, C. M. Efficient CO Oxidation at Low Temperature on Au(111). *J. Phys. Chem. B* **2006**. https://doi.org/10.1021/jp0616213.

(41) Klyushin, A. Y.; Arrigo, R.; Youngmi, Y.; Xie, Z.; Hävecker, M.; Bukhtiyarov, A. V.; Prosvirin, I. P.; Bukhtiyarov, V. I.; Knop-Gericke, A.; Schlögl, R. Are Au Nanoparticles on Oxygen-Free Supports Catalytically Active? *Top. Catal.* **2016**. https://doi.org/10.1007/s11244-015-0528-0.

(42) Mukherjee, S.; Libisch, F.; Large, N.; Neumann, O.; Brown, L. V.; Cheng, J.; Lassiter, J. B.; Carter, E. A.; Nordlander, P.; Halas, N. J. Hot Electrons Do the Impossible: Plasmon-Induced Dissociation of H_2 on Au. *Nano Lett.* **2013**, *13* (1), 240–247. https://doi.org/10.1021/nl303940z.

(43) Liu, Y.; Yan, X.; Kang, Z.; Li, Y.; Shen, Y.; Sun, Y.; Wang, L.; Zhang, Y. Synergistic Effect of Surface Plasmonic Particles and Surface Passivation Layer on ZnO Nanorods Array for Improved Photoelectrochemical Water Splitting. *Sci. Rep.* **2016**, *6* (1), 29907. https://doi.org/10.1038/srep29907.

(44) Cherevko, S.; Zeradjanin, A. R.; Keeley, G. P.; Mayrhofer, K. J. J. A Comparative Study on Gold and Platinum Dissolution in Acidic and Alkaline Media. *J. Electrochem. Soc.* **2014**, *161* (12), H822–H830. https://doi.org/10.1149/2.0881412jes.

(45) Brown, M. A.; Fujimori, Y.; Ringleb, F.; Shao, X.; Stavale, F.; Nilius, N.; Sterrer, M.; Freund, H.-J. Oxidation of Au by Surface OH: Nucleation and Electronic Structure of Gold on Hydroxylated MgO(001). *J. Am. Chem. Soc.* **2011**, *133* (27), 10668–10676. https://doi.org/10.1021/ja204798z.

(46) Plowman, B. J.; O'Mullane, A. P.; Bhargava, S. K. The Active Site Behaviour of Electrochemically Synthesised Gold Nanomaterials. *Faraday Discuss.* **2011**, *152* (0), 43. https://doi.org/10.1039/c1fd00017a.

(47) Ebrahimpour, Z.; Mansour, N. Annealing Effects on Electrical Behavior of Gold Nanoparticle Film: Conversion of Ohmic to Non-Ohmic Conductivity. *Appl. Surf. Sci.* **2017**, *394*, 240–247. https://doi.org/10.1016/J.APSUSC.2016.10.041.

(48) Pan, F.; Zhang, W.; Ye, Y.; Huang, Y.; Xu, Y.; Yuan, Y.; Wu, F.; Li, J. Adsorption Synthesis of Iron Oxide-Supported Gold Catalyst under Self-Generated Alkaline Conditions for Efficient Elimination of Carbon Monoxide. *Catalysts* **2018**.

https://doi.org/10.3390/catal8090357.

(49) Eftekharinia, B.; Moshaii, A.; Sobhkhiz Vayghan, N.; Dabirian, A. Efficient Nanoporous Hematite Photoanodes Prepared by Electron Beam Evaporation and Au Modification. *ChemCatChem* **2018**, *10* (20), 4665–4675. https://doi.org/10.1002/cctc.201800860.

(50) Nakato, Y.; Tsubomura, H. Structures and Functions of Thin Metal Layers on Semiconductor Electrodes. *J. Photochem.* **1985**, *29* (1–2), 257–266. https://doi.org/10.1016/0047-2670(85)87076-3.